Magn Reson Mater Phy (2014) 27:101–106
DOI 10.1007/s10334-013-0391-6

SHORT COMMUNICATION

Visualization of immune cell infiltration in experimental viral myocarditis by ^{19}F MRI in vivo

Christoph Jacoby · Nadine Borg · Philipp Heusch · Martina Sauter · Florian Bönner · Reinhard Kandolf · Karin Klingel · Jürgen Schrader · Ulrich Flögel

Received: 7 February 2013 / Revised: 14 June 2013 / Accepted: 17 June 2013 / Published online: 4 July 2013

Abstract
Objective This paper introduces a new approach permitting for the first time a specific, non-invasive diagnosis of myocarditis by visualizing the infiltration of immune cells into the myocardium.
Materials and methods The feasibility of this approach is shown in a murine model of viral myocarditis. Our study uses biochemically inert perfluorocarbons (PFCs) known to be taken up by circulating monocytes/macrophages after intravenous injection.
Results In vivo ^{19}F MRI at 9.4 T demonstrated that PFC-loaded immune cells infiltrate into inflamed myocardial areas. Because of the lack of any fluorine background in the body, detected ^{19}F signals of PFCs are highly specific as confirmed ex vivo by flow cytometry and histology.
Conclusion Since PFCs are a family of compounds previously used clinically as blood substitutes, the technique described in our paper holds the potential as a new imaging modality for the diagnosis of myocarditis in man.

Keywords ^{19}F MRI · Perfluorocarbons · Myocarditis · Inflammation · Macrophages

Introduction

Myocarditis, characterized by the infiltration of immune cells into myocardial tissue, is a major cause of sudden death and leads to development of both dilated and arrhythmogenic cardiomyopathies [1]. Because of the unspecific and broad spectrum of clinical signs in patients with myocarditis, diagnosis of myocarditis is still an enormous challenge [2, 3]. Gold standard for diagnosing myocarditis is yet the endomyocardial biopsy, which is invasive but currently the only method for evaluating the etiopathogenesis of inflammatory heart disease. A noninvasive diagnostic technique in the setting of acute myocarditis is contrast-enhanced cardiac MRI, but even when a combination of different acquisition techniques are used, the present MR methods lack diagnostic accuracy in controlled clinical myocarditis trails [3, 4].

Noninvasive visualization of inflammatory cells by ^{1}H MRI so far used predominantly (super)paramagnetically labeled nanoparticles taking advantage of the high affinity of these species for the monocyte–macrophage system [5–7]. Despite excellent sensitivity, this approach has the disadvantage that local deposition of these particles creates hypo/hyperintense regions in affected tissues with the entire anatomy of the investigated object as background signal, which makes an unambiguous identification in vivo difficult or even impossible. In the present study, we examined the feasibility of imaging myocarditis with a noninvasive fluorine (^{19}F) MRI approach, which we have recently shown to be suitable for visualizing the infiltration of immunocompetent cells in a variety of diseases

Electronic supplementary material The online version of this article (doi:10.1007/s10334-013-0391-6) contains supplementary material, which is available to authorized users.

C. Jacoby · N. Borg · F. Bönner · J. Schrader · U. Flögel (✉)
Department of Molecular Cardiology, Heinrich Heine University Düsseldorf, Universitätsstraße 1, 40225 Düsseldorf, Germany
e-mail: floegel@uni-duesseldorf.de

P. Heusch
Department of Diagnostic and Interventional Radiology, Heinrich Heine University Düsseldorf, Moorenstraße 5, 40225 Düsseldorf, Germany

M. Sauter · R. Kandolf · K. Klingel
Department of Molecular Pathology, Eberhard Karls University Tübingen, Liebermeisterstr. 8, 72076 Tübingen, Germany

associated with inflammation [8, 9]. For this purpose, we used emulsified perfluorocarbons (PFCs) that are biochemically inert and are preferentially phagocytized by monocytes and macrophages after intravenous injection. Because of the lack of any natural ^{19}F background, the observed signals exhibit a high degree of specificity for areas of inflammation [10].

Materials and methods

Animals

Animal experiments were performed in accordance with the national guidelines on animal care and were approved by the "Landesamt für Natur-, Umwelt- und Verbraucherschutz and the Regierungspräsidium Tübingen." Experimental myocarditis was induced in six four-week-old male ABY/SnJ mice by intraperitoneal injection of coxsackievirus B3 (CVB3) as previously described [11]. The PFC emulsion (10 % perfluoro-15-crown ether, particle size 130 nm) was prepared essentially as reported [8] and was injected intravenously (500 µl) 12 days after virus application. Animals were scanned 48 h later to allow efficient phagocytosis of the PFC label and infiltration of PFC-loaded immune cells into the infected myocardium. Six noninfected ABY/SnJ mice served as control and received the contrast agent at the same point in time.

MRI experiments

Experiments were performed at a vertical 9.4 T Bruker AVANCE^{III} Wide Bore NMR spectrometer (Bruker; Rheinstetten, Germany) operating at frequencies of 400.13 MHz for ^{1}H and 376.46 MHz for ^{19}F measurements using a Bruker Microimaging unit (Micro 2.5) equipped with an actively shielded 40-mm gradient set (1 T/m maximum gradient strength, 110-µs rise time at 100 % gradient switching), and a ^{1}H/^{19}F 25-mm birdcage resonator. After acquisition of the anatomical ^{1}H images, the resonator was tuned to ^{19}F, and morphologically matching ^{19}F images were recorded. For superimposing the images of both nuclei, the "hot iron" color lookup table (ParaVision, Bruker) was applied to ^{19}F images.

Mice were anesthetized with 1.5 % isoflurane and were kept at 37 °C. Anatomical ^{1}H images were acquired with an ECG- and respiratory-triggered fast gradient echo cine sequence (field of view [FOV], 25.6 mm × 25.6 mm; matrix, 256 × 256; slice thickness, 1 mm). Corresponding ^{19}F images were recorded from the same FOV using a multislice rapid acquisition with relaxation enhancement (RARE) sequence: RARE factor 32; TR 2.5 s; TE 5.83 ms; matrix 128 × 128; slice thickness 1 mm; averages 256; acquisition time 19.12 min. The anatomical matching multislice ^{1}H and ^{19}F MR data sets were used to quantify inflamed myocardial regions. Affected volumes were calculated from ^{19}F images by planimetric analysis of PFC signals using the region-of-interest (ROI) tool of ParaVision, multiplication with the slice thickness, and summation over all slices. For a more detailed description of MRI setup, acquisition parameters, and quantification procedures, please refer to [8, 12].

Isotropic high-resolution 3D data sets from excised hearts were acquired ex vivo from a FOV of 10 × 10 × 12.8 mm^3 using matrices of 200 × 200 × 256 for both ^{1}H and ^{19}F (acquisition time 5 h 6 min for ^{19}F). For further processing, reconstructed ^{1}H and ^{19}F image stacks were imported into the 3D visualization software Amira (Mercury Computer Systems). ^{1}H signals were associated with the respective anatomical structures using the Segmentation Editor of Amira. For segmented areas, individual surfaces were calculated with unconstrained smoothing. Subsequently, surface views with a semitransparent display using a "fancy α" were created, which enables physically correct transparencies and modifies opacity values according to their orientation with respect to the viewing direction. For overlay, anatomically corresponding ^{19}F data were volume rendered by the Voltex Module of Amira. The default color map (red) and rgba lookup mode were used for visualization, and the resulting projection from the "shining" ^{19}F data volume was computed using an intensity range of 4,000–25,000. Fade-in of the projection and concomitant rotation of the surface views were coordinated with the DemoMaker of Amira.

Flow cytometry

To validate immune cell infiltration determined by ^{19}F MRI, hearts of infected and noninfected mice ($n = 3$ each) were excised immediately after MR analysis and subjected to immune cell isolation and analysis by flow cytometry as described previously [13]. To identify the individual immune cell subsets, we used a panel of antibodies against different cell-specific markers: cytotoxic T cells (CD45$^+$, CD3$^+$, CD8$^+$), T helper cells (CD45$^+$, CD3$^+$, CD4$^+$), regulatory T cells (CD45$^+$, CD3$^+$, CD4$^+$, CD25$^+$, FoxP3$^+$), B cells (CD45$^+$, CD45R(B220)$^+$), NK cells (CD45$^+$, CD49b(DX5)$^+$, NKp46$^+$), noninflammatory monocytes (CD45$^+$, CD11b$^+$, Ly6g$^-$, CD11c$^-$, Ly6c^{low}), and macrophages/DCs (APC; CD45$^+$, CD11b$^+$, Ly6g$^-$, CD11c$^+$, F4/80$^{-/+}$).

Results

The heart was localized by acquisition of fast gradient echo ^{1}H MR cine movies, and subsequently, anatomically matching ^{19}F MR images were recorded for tracking of the

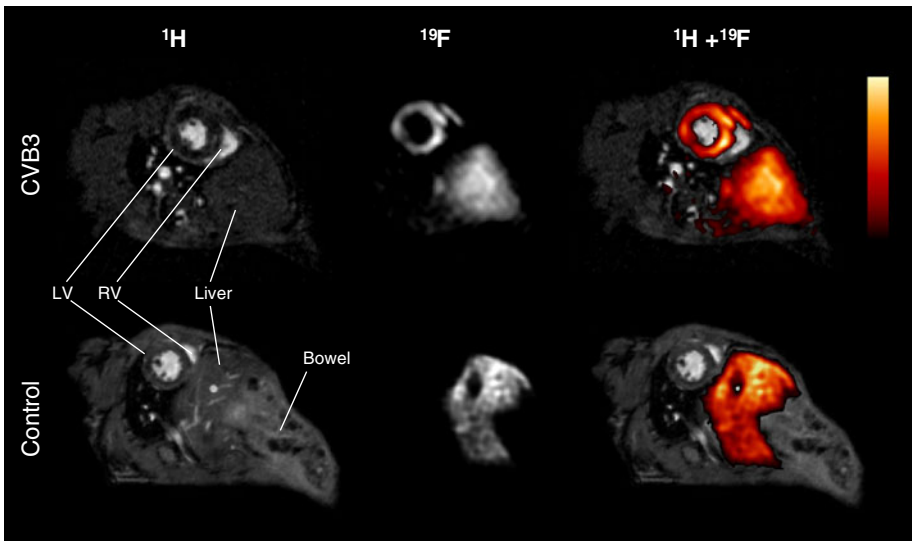

Fig. 1 In vivo ^{19}F MRI aptly visualizes myocarditis induced by coxsackievirus B3. Anatomically corresponding short-axis ^{1}H and ^{19}F MR images (field of view 25.6 mm × 25.6 mm; slice thickness 1 mm) from a ABY/SnJ mouse thorax 14 days after inducing myocarditis by injection of CVB3 and 2 days after application of PFCs (*top row*). Merged images (*right*) clearly show a homogenous accumulation of PFCs within the left ventricular wall, whereas without infection at no time were ^{19}F signals observed within the heart (*bottom*). For superimposing the images of both nuclei, the "hot iron" color lookup table (ParaVision, Bruker) was applied to ^{19}F images; *LV* left ventricle, *RV* right ventricle

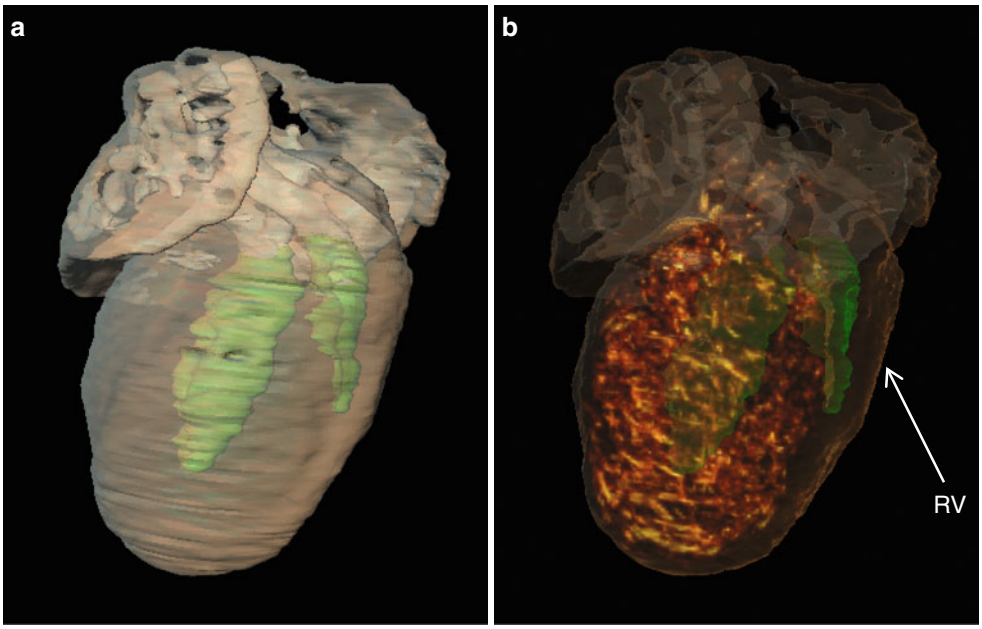

Fig. 2 High-resolution 3D ^{1}H and ^{19}F MR data sets acquired ex vivo. Reconstruction of a murine heart from isotropic ^{1}H and ^{19}F MR data sets (voxel size 0.125 nl) confirmed the prevalent confinement of the ^{19}F signal to the left ventricular wall in CVB3-induced myocarditis. **a** Contours of the heart and left/right chambers (*green*) reconstructed from ^{1}H MRI. **b** Semitransparent surface view of (**a**) overlayed by volume rendered anatomically corresponding ^{19}F data (*red*); *RV* right ventricle

injected PFCs. A typical example of consecutively recorded ^{1}H and ^{19}F MR images is illustrated in Fig. 1 (top row). The end-diastolic short-axis ^{1}H MR image is shown on the left, and in the corresponding ^{19}F MR image (middle), a signal pattern matched the shape of the left ventricular wall. Merging of these images (right) demonstrates a uniform distribution of the ^{19}F signal (red) over the anterior, lateral, posterior, and septal walls. Interestingly, only a minor PFC deposition was observed in the right ventricle. Not surprisingly, in all animals studied, ^{19}F signal was also detected in the adjacent liver tissue, due to known uptake of nanoparticles by Kupffer cells. Note

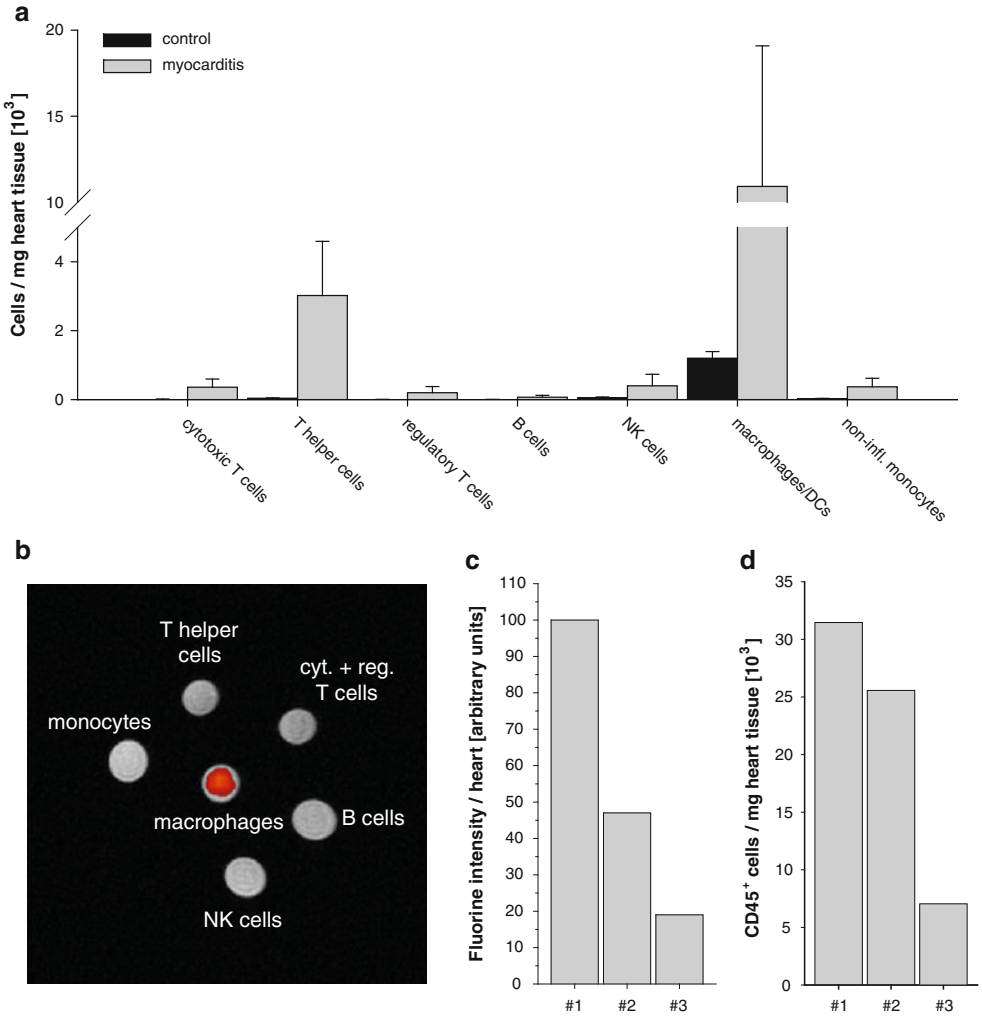

Fig. 3 Quantification of immune cells and ^{19}F signal in CVB3-infected hearts. **a** Flow cytometry after tissue digestion: immune cell subpopulations in infected and noninfected hearts ($n = 3$ each). **b** ^{1}H/^{19}F MRI of sorted immune cell subpopulations collected in 200-µl microfuge tubes: Recovery of ^{19}F label (*red*) was observed only in macrophages/DCs. Cell numbers ($\times 10^3$) were as follows: macrophages/DCs 115, T helper cells 83.3, cytotoxic and regulatory T cells 88.9, monocytes 20, and B cells 4.5. **c** Total ^{19}F MR integral determined by in vivo ^{19}F MRI and **d** number of CD45$^+$ cells in three individual hearts 14 days after infection with CVB3

that no background signal from other tissues is present. In healthy control animals at no time were ^{19}F signals observed within the heart (Fig. 1, bottom).

^{1}H/^{19}F MRIs acquired postmortem with very high resolution (Fig. 2) revealed a localized patchy PFC pattern that was homogenously distributed over the entire left ventricle. This is consistent with the local accumulation of inflammatory cells, mainly consisting of macrophages within myocardial lesions as shown by Masson's trichrome staining (myocardial lesions) and immunohistology (supplemental Figure 1). The high-resolution MRIs furthermore confirmed the in vivo results that almost no PFC deposition occured within the right ventricle (*cf.* arrow Fig. 2b; see also supplemental Movie 1). To identify the cells within the inflamed tissue that carry the ^{19}F label, hearts were enzymatically digested, and the resulting cell populations were analyzed by fluorescence-activated cell sorting (FACS). In agreement with our previous observations [11], the most prominent immune cells within CVB3-infected hearts were found to be antigen-presenting cells, comprising mainly macrophages and dendritic cells (DCs), while T lymphocytes account only for a lower amount of invading cells (Fig. 3a). This was also demonstrated by consecutive tissue sections illustrating the relationship between myocardial lesions and inflammation by detection of macrophages and CD3$^+$ T lymphocytes in infected animals (supplemental Figure 1). All sorted cell fractions were then analyzed by ^{1}H/^{19}F MRI to determine the degree of ^{19}F labeling. Figure 3b demonstrates that ^{19}F signal (red) was only found in the macrophage/DC fraction. Quantification of both the overall ^{19}F signal and the total number of infiltrated immune cells found in infected hearts

revealed that the amount of these cells was nearly reflected by the integral of the fluorine signal as determined by ^{19}F MRI in vivo (Fig. 3c, d).

Discussion

In the present study, we demonstrate in a murine model of viral myocarditis that nanoemulsions of perfluorocarbons can be used to precisely visualize focal inflammation in infected hearts as hot spots by simultaneous acquisition of morphologically matching proton (^{1}H) and fluorine (^{19}F) MR images. Injected PFCs are phagocytized primarily by circulating macrophages, resulting in ^{19}F MRI intensity signals within myocardial lesions as a result of progressive infiltration of the labeled immunocompetent cells. Although there are ex vivo reports on sequestered PFCs in healthy rat hearts [14, 15] using rather high PFC doses (50 vs. 3 mg/g body weight), long imaging times (120 vs. 20 min), and coarse voxel sizes (18 vs. 0.25 µl), we never observed in vivo ^{19}F signal in hearts of normal mice under our conditions. The patchy PFC pattern over the entire left ventricle of infected mice is consistent with the local accumulation of inflammatory cells and in good agreement with the previous histologic data on myocarditis [11]. Because of the lack of any ^{19}F background in the body, observed signals are robust, can be conveniently quantified, and exhibit an excellent degree of specificity [16, 17]. Since signal intensity in the ^{19}F images reflects the severity of inflammation, this approach is also suitable to monitor therapeutic interventions.

In contrast to conventional ^{1}H MRI diagnosis of myocarditis that relies preliminary on secondary tissue alterations such as edema, fibrosis, and necrosis [3, 4] which are rather nonspecific phenomena found to be associated with a variety of heart diseases, ^{19}F MRI specifically visualizes the recruitment of immune cells into the myocardium. The identification of this process at a time when the inflammatory cascade is just being initiated opens the possibility of early detection and more timely therapeutic intervention. Because of the biochemical inertness of perfluorocarbons and the high MR sensitivity of the fluorine nucleus that is close to that of the ^{1}H nucleus [17, 18], ^{19}F MRI may be applicable for clinical imaging of myocarditis and may represent an important step toward a rapid diagnosis and a better understanding of the pathophysiology of this disease.

Future studies will have to resolve the question whether the sensitivity of clinical scanners is sufficient for sensitive myocarditis detection. The development of dedicated ^{19}F phased-array multichannel coils and novel methods for compressed sensing acquisition could contribute to overcome signal-to-noise problems associated with the transition from small-animal MRI at high field to larger MRI scanners for human use. ^{19}F MRI in mice detects concentrations of $\approx$0.2 µmol per voxel of 0.5 $\times$ 0.5 $\times$ 1 mm^3 at 9.4 T; in humans at 3 T and employing a voxel size of 5 $\times$ 5 $\times$ 5 mm^3 in a head coil, $\approx$4 mmol would be detected with the same signal-to-noise ratio of 20 after the same acquisition duration of 20 min [19]. Thus, increasing voxel size and acquisition duration both are tools to tailor detection thresholds to accommodate the clinical question.

Conclusion

In a murine model of viral myocarditis, biochemical inert PFCs were successfully used as contrast agents for the quantitative assessment of immune cell infiltration by in vivo ^{19}F MRI, and thereby to specifically and robustly visualize the inflammatory processes that underlie this disease.

Acknowledgments This study was supported in part by the Sonderforschungsbereich 612 (JS, UF) and Transregio 19 (RK, KK), the Deutsche Forschungsgemeinschaft grant SCHR 154/13-1 (JS), and the BMBF grant 01EZ0817 (RK, KK).

Note added in proof While this paper was under review, we became aware of an independent study by van Heeswijk et al. [20] which used a similar ^{19}F MRI approach for in vivo visualization of immune cell infiltration in a murine model of autoimmune myocarditis.

References

1. Kawai C (1999) From myocarditis to cardiomyopathy: mechanisms of inflammation and cell death: learning from the past for the future. Circulation 99:1091–1100
2. Magnani JW, Dec GW (2006) Myocarditis: current trends in diagnosis and treatment. Circulation 113:876–890
3. Friedrich MG, Sechtem U, Schulz-Menger J, Holmvang G, Alakija P, Cooper LT, White JA, Abdel-Aty H, Gutberlet M, Prasad S, Aletras A, Laissy JP, Paterson I, Filipchuk NG, Kumar A, Pauschinger M, Liu P (2009) Cardiovascular magnetic resonance in myocarditis: a JACC white paper. J Am Coll Cardiol 53:1475–1487
4. Hundley WG, Bluemke DA, Finn JP, Flamm SD, Fogel MA, Friedrich MG, Ho VB, Jerosch-Herold M, Kramer CM, Manning WJ, Patel M, Pohost GM, Stillman AE, White RD, Woodard PK (2010) ACCF/ACR/AHA/NASCI/SCMR 2010 expert consensus document on cardiovascular magnetic resonance: a report of the American college of cardiology foundation task force on expert consensus documents. Circulation 121:2462–2508
5. Weissleder R, Elizondo G, Wittenberg J, Rabito CA, Bengele HH, Josephson L (1990) Ultrasmall superparamagnetic iron oxide: characterization of a new class of contrast agents for MR imaging. Radiology 175:489–493
6. Kleinschnitz C, Bendszus M, Frank M, Solymosi L, Toyka KV, Stoll G (2003) In vivo monitoring of macrophage infiltration in experimental ischemic brain lesions by magnetic resonance imaging. J Cereb Blood Flow Metab 23:1356–1361

7. Kok MB, Hak S, Mulder WJ, van der Schaft DW, Strijkers GJ, Nicolay K (2009) Cellular compartmentalization of internalized paramagnetic liposomes strongly influences both T1 and T2 relaxivity. Magn Reson Med 61:1022–1032
8. Flögel U, Ding Z, Hardung H, Jander S, Reichmann G, Jacoby C, Schubert R, Schrader J (2008) In vivo monitoring of inflammation after cardiac and cerebral ischemia by fluorine magnetic resonance imaging. Circulation 118:140–148
9. Flögel U, Su S, Kreideweiss I, Ding Z, Galbarz L, Fu J, Jacoby C, Witzke O, Schrader J (2011) Noninvasive detection of graft rejection by in vivo ^{19}F MRI in the early stage. Am J Transplant 11:235–244
10. Temme S, Bonner F, Schrader J, Flögel U (2012) ^{19}F magnetic resonance imaging of endogenous macrophages in inflammation. Wiley Interdiscip Rev Nanomed Nanobiotechnol 4:329–343
11. Klingel K, Hohenadl C, Canu A, Albrecht M, Seemann M, Mall G, Kandolf R (1992) Ongoing enterovirus-induced myocarditis is associated with persistent heart muscle infection: quantitative analysis of virus replication, tissue damage, and inflammation. Proc Natl Acad Sci USA 89:314–318
12. Ebner B, Behm P, Jacoby C, Burghoff S, French BA, Schrader J, Flögel U (2010) Early assessment of pulmonary inflammation by ^{19}F MRI in vivo. Circ Cardiovasc Imaging 3:202–210
13. Bönner F, Borg N, Burghoff S, Schrader J (2012) Resident cardiac immune cells and expression of the ectonucleotidase enzymes CD39 and CD73 after ischemic injury. PLoS One 7:e34730
14. Mason RP, Shukla H, Antich PP (1993) In vivo oxygen tension and temperature: simultaneous determination using ^{19}F NMR spectroscopy of perfluorocarbon. Magn Reson Med 29:296–302
15. Shukla HP, Mason RP, Bansal N, Antich PP (1996) Regional myocardial oxygen tension: ^{19}F MRI of sequestered perfluorocarbon. Magn Reson Med 35:827–833
16. Ruiz-Cabello J, Barnett BP, Bottomley PA, Bulte JW (2011) Fluorine (^{19}F) MRS and MRI in biomedicine. NMR Biomed 24:114–129
17. Yu JX, Kodibagkar VD, Cui W, Mason RP (2005) ^{19}F: a versatile reporter for non-invasive physiology and pharmacology using magnetic resonance. Curr Med Chem 12:819–848
18. Holland GN, Bottomley PA, Hinshaw WS (1977) ^{19}F magnetic resonance imaging. J Magn Reson 28:133–136
19. Schwitter J (2008) Extending the frontiers of cardiac magnetic resonance. Circulation 118:109–112
20. van Heeswijk RB, De Blois J, Kania G, Gonzales C, Blyszczuk P, Stuber M, Eriksson U, Schwitter J (2013) Selective in vivo visualization of immune-cell infiltration in a mouse model of autoimmune myocarditis by fluorine-19 cardiac magnetic resonance. Circ Cardiovasc Imaging 6:277–284